J. Fluid Mech. (2008), *vol.* 616, *pp.* 303–326.
doi:10.1017/S002211200800400X Printed in the United Kingdom

Energy balances for axisymmetric gravity currents in homogeneous and linearly stratified ambients

MARIUS UNGARISH[1] AND HERBERT E. HUPPERT[2]

[1]Department of Computer Science, Technion, Haifa 32000, Israel

[2]Institute of Theoretical Geophysics, Department of Applied Mathematics and Theoretical Physics, University of Cambridge, Wilberforce Rd, Cambridge CB3 0WA, UK

(Received 25 September 2007 and in revised form 29 July 2008)

We analyse the exchange of energy for an axisymmetric gravity current, released instantaneously from a lock, propagating over a horizontal boundary at high Reynolds number. The study is relevant to flow in either a wedge or a full circular geometry. Attention is focused on effects due to a linear stratification in the ambient. The investigation uses both a one-layer shallow-water model and Navier–Stokes finite-difference simulations. There is fair agreement between these two approaches for the energy changes of the dense fluid (the current). The stratification enhances the accumulation of potential energy in the ambient and reduces the energy decay (dissipation) of the two-fluid system. The total energy of the axisymmetric current decays considerably faster with distance of propagation than for the two-dimensional counterpart.

1. Introduction

Gravity currents occur whenever fluid of one density flows primarily horizontally into fluid of a different density. Many such situations arise in both industrial and natural settings, as reviewed by Simpson (1997) and Huppert (2000, 2006). Various important features of these processes have now been fairly well investigated. Our aim here is primarily to elucidate the energy flow during the propagation of high-Reynolds-number currents, such as those resulting from the instantaneous release of finite volumes of constant-density fluids over a horizontal boundary. We are particularly interested in effects due to a continuously stratified ambient. Applications of our work include areas such as oceanography, atmospheric winds and environmental control. For example, submarine wakes in oceans, contrails in the atmosphere, and the crests of lee waves in air streams over a mountain are typically regions of 'mixed' fluid whose density difference from the ambient produces a driving force of the type considered here, for example see Wu (1969).

The study of gravity currents and intrusions into a continuously stratified ambient has made significant progress in the last few years. Earlier works aimed at the elucidation of the high-Reynolds-number motion of a fixed volume of fluid released instantaneously from a lock were concerned mostly with intrusions at the level of neutral buoyancy (Wu 1969; Kao 1976; Manins 1976; Amen & Maxworthy 1980; Faust & Plate 1984; de Rooij 1999). (Related investigations concerning the waves produced in the ambient have been presented by Schooley & Hughes 1972;

Maxworthy 1980, 1983; Flynn & Sutherland 2004, but this phenomenon is beyond the scope of the present work.) The pertinent theoretical interpretations, based on box models with adjustable parameters, were found to have a quite restricted range of applicability. For example, Faust & Plate (1984) on the basis of careful comparisons with their experimental data, concluded that 'intrusions into a linearly stratified environment behave very differently from theoretical calculations'.

A turning point came with the work of Maxworthy *et al.* (2002). They considered the propagation of a saline current released from behind a lock over a horizontal bottom into a linearly stratified saline ambient in a rectangular container whose upper boundary was open to the atmosphere. The density of the current, ρ_c, was larger than, or equal to, that of the ambient at the bottom, ρ_b (the 'intrusion' corresponds to the particular case $\rho_c = \rho_b$). The investigation was a combination of laboratory and numerical experiments. Maxworthy *et al.* (2002) observed that the speed of propagation is time independent for a significant period after release (following a short adjustment interval). They obtained a quite general empirical correlation of the experimental data for this slumping velocity as a function of two governing dimensional parameters: S, which expresses the strength of the stratification, and H, which expresses the depth ratio of the ambient to the lock. Maxworthy *et al.* (2002) also provide data on the 'criticality' of the speed (with respect to the fastest internal wave in the ambient) and the position where the first significant wave–nose interaction is observed.

Motivated by the lack of theoretical interpretation of the careful observations of Maxworthy *et al.* (2002), Ungarish & Huppert (2002, 2004) and Ungarish (2005*a*) developed and verified the corresponding one-layer inviscid shallow-water formulation. This theory is based on rigorous volume and momentum balances, which are reduced to a hyperbolic system of equations for the thickness h and velocity u of the current as functions of x (the horizontal distance) and t (time), amenable to realistic initial and boundary conditions, without using any adjustable parameters. Extensions of this shallow-water formulation to the prediction of the propagation of axisymmetric and rotating currents were developed and the parameters which govern the stratification–Coriolis interactions were derived. Extensions to the flow of intrusions were presented by Ungarish (2005*b*). The new results are in very good agreement with the measurements of Faust & Plate (1984), thus resolving the dilemma of the incompatibility between theory and experiment pointed out by these authors. The new results also clarified the previously overlooked differences between intrusions released from behind a rectangular lock (Amen & Maxworthy 1980; de Rooij 1999) and a cylinder lock (Wu 1969), and proved that the propagation is always sub-critical in a linearly stratified ambient (the last result strengthens an earlier approximate deduction by Flynn & Sutherland 2004). The propagation with $t^{1/2}$, indicated by the experiments of Wu, turns out to be a similarity solution of the shallow-water balances. Ungarish (2006) generalized the nose Froude and dissipation analysis of Benjamin (1968) to a linearly stratified ambient, and showed that the classical unstratified results are fully recovered in the limit $S \to 0$.

The behaviour of the energy of the current (or intrusion) in a linearly stratified ambient is also an important issue for understanding the interaction between the current and the ambient and the behaviour of various natural hazards. In particular, it is important to clarify what is the influence of stratification on the behaviour of the energy of the current; and whether the one-layer shallow-water model, which neglects motion in the ambient, reproduces well the energy budgets of the current. A study for the two-dimensional geometry was presented by Ungarish & Huppert (2006). The

results were encouraging: the shallow-water one-layer model provided quite sharp insights into the influence of the linear stratification on the time-dependent energy budgets of the dense fluid. Navier–Stokes simulations (without turbulence closures) corroborated these predictions, and provided additional information on the energy of the ambient.

The object of this paper is to extend the investigation to an axisymmetric geometry. This has both practical and academic motivations. In various natural and industrial applications gravity currents and intrusions can propagate in an unrestricted (fully cylindrical) manner, or in an expanding wedge. There are significant qualitative and quantitative differences between the two-dimensional and axisymmetric currents (see Patterson *et al.* 2006 and Ungarish 2007 where other references are also given). For example, the two-dimensional currents display a slumping stage of propagation with constant speed, while the speed of an axisymmetric current decays from the beginning; also, the ratio of inertial to viscous effects decays much faster in an axisymmetric geometry. An axisymmetric intrusion develops a peculiar self-similar propagation in which all the dense fluid is in a ring of constant inner-to-outer radius ratio of about 0.5; this has no counterpart in the two-dimensional geometry (Ungarish & Zemach 2007; Zemach & Ungarish 2007). Moreover, the numerical simulation of the axisymmetric current is still a challenge. There is evidence that numerical simulations with a fairly large number of discretization points reproduce successfully the initial motion, up to about 2.5 to 3 lock lengths, but then the simulated current is significantly slower than experimental observations, and even becomes incoherent (Hallworth, Huppert & Ungarish 2001; Patterson *et al.* 2006). The remedy is still unclear; at present, only fully three-dimensional computations seem to be able to overcome this difficulty (Cantero, Balachandar & Garcia 2007), but these simulations are very expensive and slow. For this problematic range the shallow-water predictions are the only available practical theoretical tool (see Ungarish 2007).

It is clear that the energy behaviour of the axisymmetric current requires a dedicated investigation. A combined analytical and numerical attempt in this direction is presented in this paper.

To our knowledge, there are no previous investigations on the time-dependent energy behaviour in this configuration. The related analytical investigations of the energy of steady lenses in a rotating fluid (Stegner, Bouruet-Aubertot & Pichon 2004 and Ungarish & Huppert 2004) are relevant only to the final stages of adjustment of a current when Coriolis effects are dominant. There are no relevant experimental investigations for this geometry, to our knowledge. We hope that our results will be used for laboratory verification and extensions, in particular concerning the wave energy in the stratified media. Related works on the energy budgets of gravity currents which propagate into a homogeneous ambient were presented by Necker *et al.* (2005), Shin, Dalziel & Linden (2004) and Ungarish (2008). The first work is a careful numerical investigation, based on a high-resolution code, which focuses on the effects of particle-driven currents. The second uses a box model and various simplifications which restrict its applicability to very short distances of propagation and shallow ambients. The third paper presents a more general analysis of energy balances of two-layer models for gravity currents (and in particular clarifies the advantages and disadvantages of 'dissipative' and 'energy-conserving' approximations). We emphasize that these investigations were for a two-dimensional geometry only.

The system under consideration is sketched in figure 1: a deep layer of ambient fluid, of density $\rho_a(z)$, lies above a horizontal surface at $z = 0$. Gravity acts in the negative z-direction. The system is cylindrical about the z-axis, either as a full circle, or as a

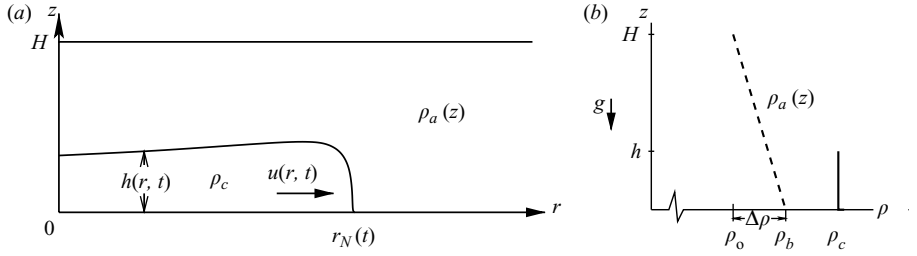

FIGURE 1. Schematic description of the system: (*a*) the geometry; and (*b*) the density profiles in the current (solid line) and ambient (dashed line).

wedge bounded by vertical, smooth, impermeable surfaces. The current propagates in the radial r-direction. At time $t=0$ a given volume of homogeneous fluid of density $\rho_c \geqslant \rho_a(0) \equiv \rho_b$ and kinematic viscosity ν, initially at rest in a cylinder of height h_0 and radius r_0, is instantaneously released into the ambient fluid. An axially symmetric current starts to spread. We assume that the Reynolds number of the horizontal flow, Re, defined below, is large, and hence viscous effects can be neglected. (After a significant spread of the current, when both its thickness and velocity are reduced, viscous forces become important. This phase is outside the scope of the present work.)

The investigation is based on a combination of shallow-water (SW) and Navier–Stokes (NS) solutions. The structure of the paper is as follows. In § 2 the energy balances are developed, first in the SW model and then in the NS formulation. A criterion for the validity of the inviscid assumption is also introduced. In § 3 we present results and comparisons of the SW and NS calculations for typical configurations. These comparisons and related discussions indicate that that, overall, the SW model captures fairly well the features of the energy transfers. In § 4 we present some concluding remarks about the effects of stratification. We also claim that the stratification of the ambient enhances the potential (wave) energy accumulation, and hence is expected to reduce the viscous dissipation (which acts on a reduced amount of kinetic energy).

2. Formulations

The configuration is sketched in figure 1. We use a cylindrical coordinate system, with the radial coordinate r along the horizontal bottom and z pointing upward. The radial and vertical velocity components are u and w. We assume that the flow does not depend on the azimuthal coordinate and that there is zero velocity in this direction. This is appropriate for the description of flow in a wedge or in a full circular geometry.

Initially, the height of the propagating current is h_0, its radius r_0 and its density ρ_c. The height of the ambient fluid is H (dimensional). The ambient fluid is stably stratified: the density at the top (usually an open boundary) is ρ_o, and it increases linearly with depth by the increment $\Delta\rho$ to the value ρ_b at the bottom. We consider situations with $\rho_b \leqslant \rho_c$.

It is convenient to use ρ_o as the reference density and to introduce the reduced density differences and ratios between them (Ungarish & Huppert 2002):

$$\epsilon = (\rho_c - \rho_o)/\rho_o, \quad \epsilon_b = (\rho_b - \rho_o)/\rho_o = \Delta\rho/\rho_o \tag{2.1}$$

and

$$S = \epsilon_b/\epsilon\,, \tag{2.2}$$

from which it follows that

$$\rho_c = \rho_o(1+\epsilon), \quad \rho_a = \rho_b - \frac{\Delta\rho}{H}z = \rho_o\left[1+\epsilon\, S\left(1-\frac{z}{H}\right)\right]. \tag{2.3}$$

The parameter S represents the magnitude of the stratification in the ambient fluid, and we consider only $0 \leqslant S \leqslant 1$. The homogeneous ambient is recovered by setting $S=0$. We also define the reference reduced gravity,

$$g' = \epsilon\, g, \tag{2.4}$$

where g is the gravitational acceleration.

We recall that the buoyancy frequency is defined by

$$\mathcal{N}^2 = g\Delta\rho/(\rho_o H) = g'S/H, \tag{2.5}$$

and that the leading, or mode-one, linear internal wave in a closed two-dimensional channel propagates with velocity (Baines 1995)

$$u_W = \pm\mathcal{N}H/\pi. \tag{2.6}$$

It is convenient for purposes of interpretation to keep in mind the following picture: $S=0$ corresponds to a homogeneous ambient of density ρ_o and a current of density ρ_c. For $0<S<1$ the density of the ambient is stratified (increases linearly) from the same ρ_o at the top to a larger density at the bottom. The extreme situation $S=1$ is achieved when the density of the ambient at the base matches that of the current.

We note that the $S=1$ case also describes a symmetric intrusion which propagates at the level of neutral buoyancy. The inviscid Boussinesq current considered here makes up the upper half of this intrusion, and the lower part is just its mirror image. To achieve a similar mirror symmetry in the ambient, we must assume that the neutral buoyancy level is at the middle of the container. (For more details on the flow field see Ungarish & Zemach 2007.)

2.1. *SW model*

We shall use a one-layer approximation which omits the motion in the ambient. This is the simplest shallow-water model. Actually, the propagation of the current at the bottom must produce a return flow in the ambient above. Experimental and numerical results (Wu 1969; Maxworthy *et al.* 2002; Ungarish & Huppert 2004; Ungarish 2005*b*; Ungarish & Zemach 2007) show that this flow has a quite complex z-dependence. Therefore, in contrast with the unstratified case, the flow field in the stratified ambient cannot be directly expressed by averaged variables. A reliable two-layer model for the stratified configuration is still lacking. Thus, although the one-layer model represents a bold simplification, at present it is the only available framework of governing equations for analytical investigation. Previous studies indicated that this model captures well many of the important features of the flow in both two-dimensional and axisymmetric geometries. This justifies the use of this model for the energy calculations in the present problem.

To be specific, we assume that in the ambient fluid domain the velocity is zero and hence the fluid is in purely hydrostatic balance and maintains the initial density $\rho_a(z)$ given by (2.3). Motion is assumed to take place in the lower layer only, $0 \leqslant r \leqslant r_N(t)$ and $0 \leqslant z \leqslant h(r,t)$, see figure 1. As in the classical inviscid shallow-water analysis

of a gravity current in a homogeneous ambient, we argue that the predominant vertical momentum balance in the current is hydrostatic and that viscous effects in the horizontal momentum balance are negligibly small (the quantitative criteria will be specified later in § 2.1.2). Hence the motion is governed by a balance between pressure and inertial forces in this horizontal direction. As in the situation with a homogeneous ambient, an order-of-magnitude analysis indicates that the perturbation of the upper free surface introduced by the flow can be neglected when $\epsilon \ll 1$, as assumed here.

A relationship between the pressure fields and the height $h(r, t)$ can be obtained. The hydrostatic balances are $\partial p_i/\partial z = -\rho_i g$, where $i = a$ or c, and in the motionless ambient the pressure does not depend on r. Use of (2.3) then yields

$$p_a(z, t) = -\rho_o \left[1 + \epsilon\, S\left(1 - \frac{1}{2}\frac{z}{H}\right)\right] gz + C, \tag{2.7}$$

$$p_c(r, z, t) = -\rho_o(1 + \epsilon\,)gz + f(r, t), \tag{2.8}$$

where C is a constant. Pressure continuity between the ambient and the current on the interface $z = h(r, t)$ determines the function $f(r, t)$ of (2.8) and we obtain, after some algebra,

$$p_c(r, z, t) = -\rho_o(1 + \epsilon\,)gz + \rho_o g' \left[h - S\left(h - \frac{1}{2}\frac{h^2}{H}\right)\right] + C, \tag{2.9}$$

and consequently

$$\frac{\partial p_c}{\partial r} = \rho_o g' \frac{\partial h}{\partial r}\left[1 - S\left(1 - \frac{h}{H}\right)\right]. \tag{2.10}$$

This relationship between $\partial p_c/\partial r$ and $h(r, t)$ allows us to eliminate the pressure from the radial momentum balance and to obtain the SW equations as a hyperbolic system for $h(r, t)$ and $u(r, t)$. The equations of motion will be presented in § 2.1.2. We shall first consider the energy terms in this model.

2.1.1. *Energy*

In the SW framework the speed of motion is represented by the z-independent average horizontal velocity, and hence the kinetic energy of the current (denoted by subscript c) is given by

$$K_c(t) = \frac{1}{2}\rho_c \int_0^{r_N(t)} u^2(r, t)h(r, t)r\,\mathrm{d}r. \tag{2.11}$$

The vertical displacement of the dense fluid particles is resisted by the hydrostatic pressure of the surrounding ambient fluid. The resulting buoyancy acceleration is $[\rho_c - \rho_a(z)]g$ and the corresponding work needed to move a unit volume from the bottom to some z, in the present linear density profile $\rho_a(z)$, is $g[(\rho_c - \rho_b)z + (1/2)\Delta\rho\, z^2/H]$. The potential energy of the current is therefore

$$\begin{aligned} P_c(t) &= g \int_0^{r_N(t)} r\,\mathrm{d}r \int_0^{h(r,t)} \left[(\rho_c - \rho_b)z + \frac{1}{2}\frac{\Delta\rho}{H}z^2\right] \mathrm{d}z \\ &= g \int_0^{r_N(t)} \left[\frac{1}{2}(\rho_c - \rho_b)h^2 + \frac{1}{6}\frac{\Delta\rho}{H}h^3\right] r\,\mathrm{d}r. \end{aligned} \tag{2.12}$$

Initially, at $t=0$, $h=h_0$, $r_N=r_0$ and $u=0$. Consequently, $K_c(0)=0$ and, using (2.1)–(2.4), we obtain

$$P_c(0)=\left(\frac{1}{4}\rho_o r_0^2 h_0^2 g'\right)\left[1-S+\frac{1}{3}\frac{S}{H/h_0}\right]. \tag{2.13}$$

This indicates that energy in the problem under investigation is conveniently scaled with $(\rho_o r_0^2 h_0^2 g')/4$, as is done in (2.14). For a particular system it is convenient to refer the energy to $P_c(0)$, as is done in §§ 3 and 4.

2.1.2. *Governing SW equations*

It is convenient to scale the dimensional variables (denoted here by asterisks) by

$$\{r^*, z^*, h^*, H^*, t^*, u^*, E^*\}=\{r_0 r, h_0 z, h_0 h, h_0 H, Tt, Uu, (1/4)\rho_o U^2 h_0 r_0^2 E\}, \tag{2.14}$$

where

$$U=(h_0 g')^{1/2} \quad \text{and} \quad T=r_0/U. \tag{2.15}$$

Here h_0 and r_0 are the initial height and length of the current, U is a typical inertial velocity of propagation of the nose of the current and T is a typical time period for longitudinal propagation over a typical distance r_0. The variable E denotes the energy (per radian of azimuthal angle). Note that the horizontal and vertical lengths are scaled differently, which removes the initial aspect ratio h_0/r_0 from the SW analysis in the homogeneous case (Ungarish & Huppert 1999), and this applies also to the stratified case considered here. A representative Reynolds number of the current is defined as $Re=Uh_0/\nu$, where ν is the kinematic viscosity, assumed constant in the system.

The relevant volume and momentum balances have been developed and verified in previous investigations (Ungarish & Huppert 2002, 2004; Ungarish 2005*a*). Here we briefly mention the equations used in the present work.

In conservation form, the continuity and momentum equations can be written as

$$\frac{\partial h}{\partial t}+\frac{\partial}{\partial r}(ruh)=0 \tag{2.16}$$

and

$$\frac{\partial}{\partial t}(uh)+\frac{\partial}{\partial r}\left[u^2 h+\frac{1}{2}(1-S)h^2+\frac{1}{3}S\frac{h^3}{H}\right]=-\frac{u^2 h}{r}. \tag{2.17}$$

Following the standard procedure, we calculate the speeds of propagation of the characteristics

$$\lambda_{\pm}=u\pm\left[h\left(1-S+S\frac{h}{H}\right)\right]^{1/2}. \tag{2.18}$$

On $\mathrm{d}r/\mathrm{d}t=\lambda_{\pm}$, the dependent variables satisfy

$$\mathrm{d}h\pm\left[\frac{1-S+S(h/H)}{h}\right]^{-1/2}\mathrm{d}u=-\frac{uh}{r}\mathrm{d}t. \tag{2.19}$$

The initial conditions are zero velocity and unit dimensionless height and length at $t=0$. Also, the velocity at the axis $r=0$ is zero, and an additional condition is needed at the nose $r=r_N(t)$. As in previous investigations (Ungarish & Huppert 2002, 2004; Ungarish 2005*a*), we write

$$u_N=Fr\,h_N^{1/2}\left[1-S\left(1-\frac{1}{2}\frac{h_N}{H}\right)\right]^{1/2}. \tag{2.20}$$

Here the Froude number Fr expresses the ratio of the velocity of propagation of the nose, u_N, to the effective pressure head (per unit mass) at the nose whose thickness is h_N. The term in the square brackets of (2.20) is equal to 1 in the non-stratified case ($S=0$), and smaller than 1 for $S>0$. This term indicates the explicit slowing of the head due to stratification effects. We argue that the effective Fr is a function of h_N/H only, and the practical numerical value is well approximated by the simple semi-empirical correlation of Huppert & Simpson (1980)

$$Fr = \begin{cases} 1.19 & (0 \leqslant h_N/H \leqslant 0.075) \\ 0.5\,(h_N/H)^{-1/3} & (0.075 \leqslant h_N/H \leqslant 1). \end{cases} \tag{2.21}$$

Ungarish (2006) presented a generalization of the classical analysis of Benjamin (1968) to the linearly stratified ambient. These more rigorous results also show that (2.20) and (2.21) are a good approximation for a current released instantaneously from behind a lock into a linearly stratified ambient. Strictly speaking, these justifications were derived for a two-dimensional flow. However, in the framework of the SW formulation the nose is treated as a thin jump, and hence the curvature terms of the present cylindrical geometry are unimportant. We therefore adopt (2.21) as a prototype correlation in the following study, but it will be evident that the essence of the analysis and conclusions are not affected by the details of the functional form of $Fr(h_N/H)$.

The effect of viscous friction on the motion of the current increases with time and distance of propagation. Even for quite large values of Re, the inviscid SW formulation may become invalid at moderate values of r_N. This tendency is enhanced by stratification as shown below. To monitor this effect, we use the previous results for u and h to estimate the time-dependent ratio of global inertial, F_I, to viscous, F_V, effects. Since the inertia per unit volume is well represented by $\rho_c u u_r$, and the viscous force per unit area is expected to be proportional to $\rho_o \nu u/h$ we obtain, in dimensionless form,

$$\frac{F_I}{F_V} \approx Re\frac{h_0}{r_0}\frac{\displaystyle\int_0^{r_N(t)} uu_r hr\,\mathrm{d}r}{\displaystyle\int_0^{r_N(t)} (u/h)r\,\mathrm{d}r} = Re\frac{h_0}{r_0}\theta(t). \tag{2.22}$$

The function $\theta(t)$ is expected to be of the order of unity at the beginning of the propagation and decay to quite small values. This function can be easily calculated from the SW results for $u(r,t)$ and $h(r,t)$, but can also be estimated analytically using box-model considerations as follows.

Assuming that the current is a cylinder box of height $h_N(t)$, and accordingly $u = u_N r/r_N$, we obtain $\theta \approx u_N h_N^2 r_N^{-1}$. The value of u_N is estimated from (2.20) and (2.21) as: (*a*) $[(1-S)h_N]^{1/2}$ for S not close to 1; and (*b*) $h_N/H^{1/2}$ for $S \approx 1$. In this estimate we consider Fr to be a constant because the current is expected to be thin when viscous effects are relevant. Finally, we use volume conservation to obtain $h_N = 1/r_N^2(t)$. This yields

$$\theta \approx \begin{cases} (1-S)^{1/2} r_N^{-6} & (S \text{ not close to } 1) \\ H^{-1/2} r_N^{-7} & (S \approx 1). \end{cases} \tag{2.23}$$

Using these results, we can estimate the importance of the viscous terms, and also the limit of validity of the inviscid assumption, for a real gravity current with given Re and h_0/r_0. The inviscid theory is expected to be relevant for, roughly, $F_I/F_V > 3$. The stratification enhances the effect of viscosity. The contribution of the viscous

terms increases very fast with the radius of propagation, in particular when S is close to 1. The transition from inertial to viscous dominance is not a clear-cut experimental observation, because is is expected to occur gradually, first in the thinner layer of fluid near the centre and later in the thicker front domain. The cases discussed in this study are in the inertia-dominated regime. We recall that for the two-dimensional current the first and second lines of (2.23) show decay with $x_N^{-7/2}$ and x_N^{-4}, respectively, where x_N is the counterpart of r_N. The axisymmetric current is more prone to viscous influence because its thickness decreases like r_N^{-2}.

2.2. *Navier–Stokes considerations*

We consider, again, an axisymmetric cylindrical domain with velocity $\boldsymbol{v} = u\hat{\boldsymbol{r}} + w\hat{\boldsymbol{z}}$. We employ the following dimensional balance equations.

1. Conservation of volume

$$\nabla \cdot \boldsymbol{v} = 0. \tag{2.24}$$

2. Momentum balance

$$\rho \frac{\mathrm{D}\boldsymbol{v}}{\mathrm{D}t} = -\nabla p - (\rho - \rho_b) g \hat{\boldsymbol{z}} + \mu \nabla^2 \boldsymbol{v}, \tag{2.25}$$

where p is the pressure reduced with $\rho_b g z$ and μ is the dynamic viscosity coefficient, assumed constant and equal for both fluids.

3. Density transport

$$\frac{\mathrm{D}\rho}{\mathrm{D}t} = 0. \tag{2.26}$$

In the numerical computations a small diffusion term, $\kappa \nabla^2 \rho$, was added to the right-hand side of (2.26). This was done for smoothing purposes, but its effect on the results is within the bounds of the numerical truncation errors.

For energy considerations, we multiply the horizontal and vertical components of (2.25) by u and w, respectively and add the results. After some algebra and use of (2.24), we obtain

$$\rho \frac{\mathrm{D}}{\mathrm{D}t}\left[\frac{1}{2}(u^2 + w^2)\right] = -\nabla \cdot p\boldsymbol{v} - (\rho - \rho_b) g w + \Phi, \tag{2.27}$$

where $\Phi = \mu \boldsymbol{v} \cdot \nabla^2 \boldsymbol{v}$, is the standard viscous dissipation function for the Navier–Stokes formulation.

Consider the integral of (2.27) over the volume Ω of the two-fluid system. For simplicity, we consider a closed cylindrical domain $0 \leqslant r \leqslant r_{\mathrm{w}}, 0 \leqslant z \leqslant H$. This domain Ω is the union of Ω_c (for the current) and Ω_a (for the ambient fluid). Within the Boussinesq approximation $O(\epsilon)$ error bounds, the slightly varying ρ on the left-hand side can be replaced by the constant ρ_o. The integrated left-hand-side term thus yields the rate of change of the total kinetic energy, defined by

$$K_i(t) = \rho_o \int_{\Omega_i} \frac{1}{2}(u^2 + w^2)\, \mathrm{d}V, \tag{2.28}$$

where i is a for the ambient, c for the current, and no subscript for the whole system. On the right-hand side, the integrated contribution of the pressure term vanishes on account of the boundary conditions. The effect of the dissipation term on the time-dependent energy behaviour of the system enters via

$$\mathscr{D}(t) = \int_0^t \mathrm{d}t \int_{\Omega} \Phi \, \mathrm{d}V. \tag{2.29}$$

The integral of the second term on the right-hand side of (2.27), which represents the work of the buoyancy force, can be manipulated into an informative form as follows. We introduce the vertical upward displacement $\eta(r, z, t)$ of a particle of density ρ in the ambient fluid from its initial position in the linear density profile. The conservation of density of the particle, combined with (2.3), yields

$$\eta(r, z, t) = z - [\rho_b - \rho(r, z, t)]\, H/\Delta\rho. \tag{2.30}$$

Consequently,

$$\begin{aligned}\int_\Omega g(\rho - \rho_b) w \mathrm{d}V &= g \int_{\Omega_c} \left(\rho_c - \rho_b + \frac{\Delta\rho}{H} z - \frac{\Delta\rho}{H} z\right) w \mathrm{d}V \\ &\quad + g \int_{\Omega_a} \left[\rho_b - \frac{\Delta\rho}{H}(z - \eta) - \rho_b\right] w \mathrm{d}V \\ &= \frac{\mathrm{D}}{\mathrm{D}t}\left[g \int_{\Omega_c} \left[(\rho_c - \rho_b) z + \frac{1}{2}\frac{\Delta\rho}{H} z^2\right] \mathrm{d}V\right] + \frac{\mathrm{D}}{\mathrm{D}t}\left[\rho_o\, \mathscr{N}^2 \int_{\Omega_a} \frac{1}{2}\eta^2 \mathrm{d}V\right] \\ &\quad - g\frac{\Delta\rho}{H} \int_\Omega z w \,\mathrm{d}V,\end{aligned} \tag{2.31}$$

where the definition (2.5) of $\mathscr{N}$ and the continuity equation (2.26) were also used. The last term on the right-hand side vanishes because of the velocity boundary conditions. The first and second terms represent the rate of change of the potential energy of the current and ambient, respectively. If mixing and turbulence are important, a more complex energy-budget analysis is required; in particular, the method suggested by Winters *et al.* (1995) seems appropriate for this extension. In this study we focus our attention on the fundamental forms of energy transfers in an idealized gravity current system, and this is conveniently described by the present simplified balances.

Hereafter, dimensionless variables are used unless stated otherwise. The scaling is provided by (2.14); in particular, the energy is scaled with $(1/4)\rho_o r_0^2 h_0^2 g'$ and η with h_0.

As expected, the energy terms for the current are similar to these derived for the SW case. In the SW approximation the contribution of w to the kinetic energy has been discarded. According to (2.31), the second term on the right-hand side, the scaled form of the potential energy of the ambient is

$$P_a(t) = 2\frac{S}{H} \int_{\Omega_a} \eta^2 \,\mathrm{d}V. \tag{2.32}$$

This indicates that for weak stratification (small S) most of the energy transferred to the ambient is of kinetic type, and hence more prone to viscous dissipation. This trend is consistent with the observation of Necker *et al.* (2005) that higher levels of kinetic energy are associated with larger values of viscous dissipation.

We are concerned with the behaviour of the mechanical energies; total energy refers to the sum of kinetic and potential components. The total energy of the two-fluid system is expected to decay due to irreversible viscous dissipation.

The numerical solution of the NS axisymmetric formulation was obtained by using a finite-difference method which provides the values of u, w and ρ on a fixed r, z-grid. The details of this numerical numerical code are as reported in Ungarish & Huppert (2004); for the present work, the same code was extended for the calculation of the energy terms. The propagation predictions of this code were compared in previous works with non-stratified experiments and SW results. For example, consider the

case S3 displayed in figure 10 in Hallworth *et al.* (2001). We see that, as mentioned previously, the NS results are in good agreement with the experiment for about $r_N = 3$; then, the finite-difference current lags behind the experimental data, but the SW current remains in good agreement for a significantly longer distance. Such comparisons for stratified ambients could not be performed because no reliable experimental data is available, to our knowledge.

For the convenience of both numerical simulation and presentation of the results, we introduce the density function $\phi(\boldsymbol{r}, t)$ defined by

$$\phi(r, z, t) = \frac{\rho(r, z, t) - \rho_o}{\rho_c - \rho_o} = \frac{1}{\epsilon}\left[\frac{\rho(r, z, t)}{\rho_o} - 1\right], \tag{2.33}$$

where ϵ is the reduced density difference given by (2.1). We expect $0 \leqslant \phi \leqslant 1$, with $\phi = 1$ in the domain of the 'pure' dense fluid and $0 \leqslant \phi \leqslant S$ in the domain of the ambient fluid.

The parameters of the numerical computation are: first, as in the SW formulation, the values of S and the (dimensionless) depth H; and, in addition, the values of $Re = (g' h_0)^{1/2} h_0 \rho_o / \mu$, ϵ, the initial aspect ratio of the dense fluid h_0/r_0, and length of the tank, r_{w} (scaled with r_0). (The coefficient of the artificial diffusion term which was added on the right-hand side of the density transport was typically $(10Re)^{-1}$. The actual Schmidt number, ν/κ, is significantly larger in a typical two-liquid system, but the physical diffusion process is beyond the resolution of the present computations.) The details will be given in § 3.2.

The initial conditions at $t = 0$ are

$$\boldsymbol{v} = \boldsymbol{0} \quad (0 \leqslant r \leqslant r_{\mathrm{w}}, \quad 0 \leqslant z \leqslant H), \tag{2.34}$$

$$\phi = \begin{cases} 1 & (0 \leqslant r \leqslant 1, \quad 0 \leqslant z \leqslant 1) \\ S(1 - z/H) & \text{elsewhere.} \end{cases} \tag{2.35}$$

The boundary conditions of the code are, briefly: the bottom and outer wall are treated as solid boundaries, the top as a shear-free impermeable fixed boundary, and at the axis $r = 0$ the radial fluxes vanish and the variables are regular.

The finite-difference results provide the values of u, w and ϕ at grid points. This allows the calculation of the potential and kinetic energies of the current and of the ambient. The values of η_{ij} (at grid points r_i, z_j) were calculated with the aid of (2.30) and (2.33) by

$$\eta_{ij} = z_j + H(\phi_{ij}/S - 1). \tag{2.36}$$

3. Results

We consider the influence of the stratification, S, on the the energy behaviour of the gravity current released from behind a lock in a configuration with $H = 3$ (dimensionless). This geometry is expected to be typical of currents in a non-shallow ambient. The parameters H and S considered here are also compatible with those used in the previous investigation of the two-dimensional current (Ungarish & Huppert 2006), which facilitates the comparison between the axisymmetric and the Cartesian geometries. The results are presented in dimensionless form subject to the scaling (2.14).

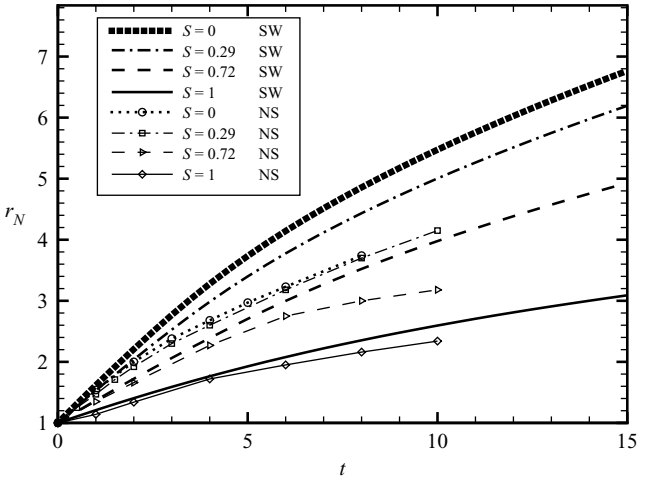

FIGURE 2. The propagation of the nose as a function of time for $H = 3$ and various values of S. SW results (curves) and NS results (curves with symbols) for various values of S.

3.1. *SW results*

In general, the SW governing equations (2.16) and (2.17) with the appropriate initial and boundary conditions must be solved numerically. For large times analytical similarity solutions for the cases $S = 0$ and $S = 1$ are available; these will be used later in this section.

The main SW results were obtained as follows. We solved the governing equations by a two-step Lax–Wendroff method (see Morton & Mayers 1994; Press *et al.* 1992). The typical grid has 500 intervals over $[0, r_N(t)]$ and a time step of 10^{-3}. The resulting discrete values of h and u were used to calculate the energy integrals (2.11) and (2.12) by the trapezoidal rule. The estimated numerical errors are less than 1%. The predicted propagation of the nose is presented in figure 2. As expected, as the stratification parameter S increases, the speed of propagation is reduced. Cases $S = 0$ and $S = 0.29$ are super-critical with respect to u_W, while $S = 0.72$ and $S = 1$ are sub-critical, see (2.6). (To be more specific, we mention that the SW values of (u_N, u_W) are $(0.54, 0.30)$ for $S = 0.29$ and $(0.38, 0.47)$ for $S = 0.72$ shortly after release.) The super- and sub-criticality of two-dimensional currents with similar initial conditions has been confirmed experimentally by Maxworthy *et al.* (2002). However, there is a significant difference between the two-dimensional and the axisymmetric cases: in the former there is a stage of propagation with constant speed for several lock lengths, while in the latter the speed decays with t from the beginning (see (2.19)). Consequently, the super-critical axisymmetric current will become sub-critical after a relatively short propagation.

Figure 3 shows the decay of the ratio of inertial to viscous effects calculated from the SW results. At the initial stages the rate of decay varies, according to the adjustment stages of the gravity current, but a constant slope (on the log-log axes) is eventually achieved. The decrease of θ when S increases, and these constant slopes confirms the estimates (2.23). The present inviscid approach is valid as long as $\theta Re(h_0/r_0)$ remains large (say > 3). Thus, for the typical value of $Re(h_0/r_0) = 10^3$, viscous effects may become dominant after a propagation to about $r_N = 3.5$ for small S and $r_N = 2.5$ for S close to 1. We shall restrict our analysis to these values. Although this is not a very significant propagation, the mean thickness of the current is reduced by a factor of

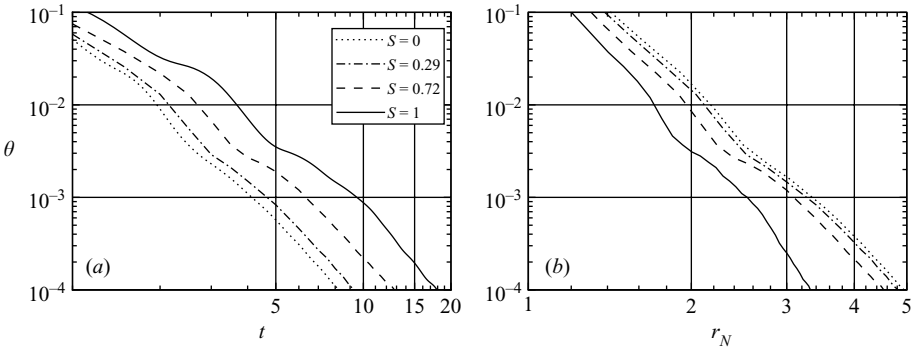

FIGURE 3. SW results. The coefficient θ, defined in (2.22), for $H = 3$ and various values of S: as a function of t (a) and of r_N (b).

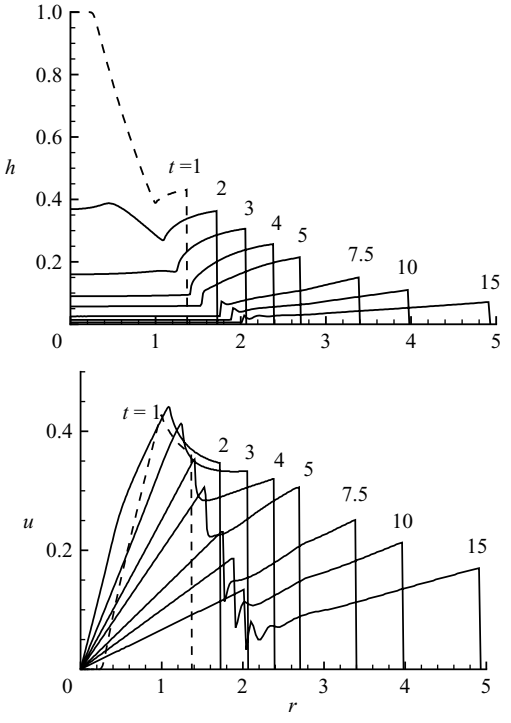

FIGURE 4. SW results. The thickness and velocity profiles for $H = 3$, $S = 0.72$, for various times.

about 10. This implies a very significant decay of the potential energy P_c, see (2.12), and hence the main process is covered.

The typical behaviour of the current as predicted by the SW solution is shown in figure 4. Both the height and the speed display a quite complex dependence on both time and radius. There is an initial 'dam-break' phase during which a backward-moving rarefaction wave sets into motion the fluid in the lock. At $t = 1$ the interface is still quite high near the centre, and there is still a core with $u = 0$. By $t = 2$ all the fluid is moving and the height of the interface is everywhere below 0.4. Next, most of the fluid is concentrated in a quite prominent external ring, followed by a thin

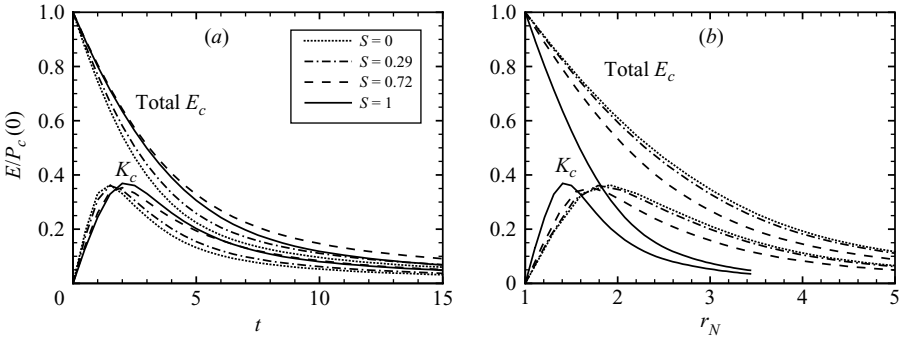

FIGURE 5. SW results. The kinetic and total energy of the current as functions of time (*a*) and r_N (*b*), for various values of S.

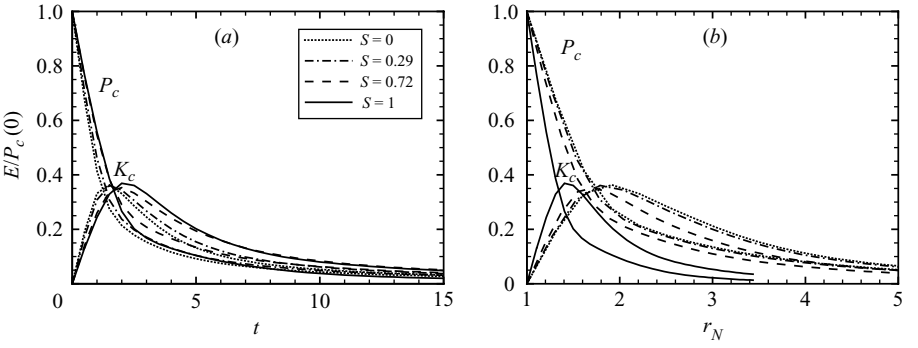

FIGURE 6. SW results. The kinetic and potential energy of the current as functions of time (*a*) and r_N (*b*), for various values of S.

horizontal tail. The velocity in this tail is quite large (the small oscillation about the sharp changes are spurious numerical effects, with insignificant contributions to the energy calculations). Eventually, the current becomes a thin layer with a slight upward inclination, and the velocity tends to a linear profile. These complex variations of h and u are expected to affect dramatically the energy exchanges of the current. Unlike the two-dimensional case, we cannot define a clear-cut slumping phase of motion with constant speed.

Figures 5 and 6 display the SW energy balances of the current as functions of time and of distance for various values of the stratification parameter S. The energies of each system are referred to the initial potential energy $P_c(0)$, see (2.13). In all cases, the potential energy decays monotonically, while the kinetic energy has an initially increasing and then decreasing profile with a maximum of about 0.4 at $t \approx 2$ to 3. These energy trends can be understood in view of the h and u profiles shown in figure 4. The kinetic energy of the current develops from zero during the 'dam-break' phase of the motion. The rarefaction wave which travels backward into the bulk of stationary fluid sets this fluid into motion and increases the kinetic energy. Then the current evolves to, roughly, a cylinder of height $h_N \approx 0.4$. This geometry contains less than half of the original potential energy. Here the kinetic energy reaches the maximum, and the kinetic and potential energy are roughly equal. Next, both the kinetic and potential energies of the current decay at about the same rate.

We note that the energy decay as a function of the distance of propagation r_N is quite insensitive to the value of S for approximately $S < 0.7$. The case $S = 1$ (i.e. $\rho_c = \rho_b$, the strongest stratification in the present framework) displays a different behaviour with r_N to the other cases: the total energy of the current, $E_c = P_c + K_c$, decays faster, and the maximum of the kinetic energy is attained after a shorter propagation. The interpretation is as follows. The total energy of the current decreases with time because of the work of pushing the nose against the ambient pressure. An estimate gives $\mathrm{d}E_c/\mathrm{d}r \approx -0.5\Delta p h_N r_N$, where Δp is the pressure difference between current and ambient at the botom of the front ($r = r_N$, $z = 0$). Using (2.7) and (2.9) we find that: (i) for S not close to 1, $[(\mathrm{d}E_c/\mathrm{d}r)/P_c(0)] \approx -h_N^2 r_N$; and (ii) for $S \approx 1$, $[(\mathrm{d}E_c/\mathrm{d}r)/P_c(0)] \approx -h_N^3 r_N$. These approximations explain the collapse of the curves $S = 0, 0.29, 0.72$, as opposed to the faster decay curve for $S = 1$, in figure 6.

We can supplement the trends derived from the numerical solution with some available analytical results of the SW equations at large t. At this stage the initial conditions are 'forgotten' except for the prescribed fixed volume $\mathscr{V}$ (per radian), and Fr has attained a constant value because h_N/H is very small. A self-similar behaviour appears for $S = 0$ and $S = 1$. The space-similarity coordinate is

$$y = r/r_N(t) = r/At^{\beta} \quad (0 \leqslant y \leqslant 1), \tag{3.1}$$

where A and β are constants defined below.

The self-similar propagation for the non-stratified $S = 0$ axisymmetric case has been well investigated (see Grundy & Rottman 1985; Huppert & Dade 1998; Zemach & Ungarish 2007). However, the corresponding energy results have not been reported before, to our knowledge. The classical results are as follows.

The solution of the equations and nose boundary condition is

$$r_N = At^{1/2}, \quad h = \dot{r}_N^2 \left[\frac{1}{Fr^2} + \frac{1}{2}(y^2 - 1)\right], \quad u = \dot{r}_N y, \tag{3.2}$$

where the overdot denotes time derivative and

$$A = 2\left(\frac{2Fr^2}{4 - Fr^2}\right)^{1/4} \mathscr{V}^{1/4}. \tag{3.3}$$

Since $\dot{r}_N = (1/2)At^{-1/2}$, (3.2) can also be expressed as

$$r_N = At^{1/2}, \quad h = \frac{1}{4}A^4 r_N^{-2}\left[\frac{1}{Fr^2} + \frac{1}{2}(y^2 - 1)\right], \quad u = \frac{1}{2}A^2 r_N^{-1} y. \tag{3.4}$$

These results cover the entire domain $0 \leqslant y \leqslant 1$.

We calculate the energy by using the definitions (2.11) and (2.12). In scaled form we obtain

$$K_c = 4r_N^2 \int_0^1 \frac{1}{2}u^2(y,t)h(y,t)y\,\mathrm{d}y = 2\left(\frac{A}{2}\right)^6 \left(\frac{1}{Fr^2} - \frac{1}{6}\right) t^{-1}, \tag{3.5}$$

$$P_c = 4r_N^2 \int_0^1 \frac{1}{2}h^2(y,t)y\,\mathrm{d}y = 2\left(\frac{A}{2}\right)^6 \left(\frac{2}{Fr^4} - \frac{1}{Fr^2} + \frac{1}{6}\right) t^{-1}, \tag{3.6}$$

$$E_c = K_c + P_c = \left(\frac{1}{2Fr}\right)^4 A^6 t^{-1}. \tag{3.7}$$

(The integrals in (3.5) and (3.6) are multiplied by 4 because of the energy scaling, see (2.14).) The conclusion is that the energy of the axisymmetric current in a

non-stratified ambient decays like t^{-1} or r_N^{-2}. In the self-similar stage $K_c > P_c$. In the present case $\mathscr{V} = 1/2$. This analytical result is in good agreement with the numerical solution of the SW equations.

For the $S = 1$ case the similarity solution presented by Ungarish & Zemach (2007) and Zemach & Ungarish (2007) is

$$r_N(t) = At^{1/3}, \quad h(y,t) = \dot{r}_N \sqrt{2H}\left(y^2 - y_1^2\right)^{1/2}, \quad u(y,t) = \dot{r}_N\, y, \tag{3.8}$$

where

$$y_1 = \left(1 - \frac{1}{Fr^2}\right)^{1/2}, \tag{3.9}$$

$$A = 3Fr\left[\frac{\mathscr{V}}{3\sqrt{2H}}\right]^{1/3}. \tag{3.10}$$

For the present value of $Fr = 1.19$ we obtain $y_1 = 0.54$. The entire volume of the dense fluid is in the ring $y_1 r_N(t) \leqslant r \leqslant r_N(t)$. It was shown in Ungarish & Zemach (2007) that an intrusion released from behind a lock indeed converges to this particular solution. In addition, there is a thin disk-tail left behind, whose volume is small compared with that in the ring and decays like $t^{-4/3}$.

We calculate the energy by using the definitions (2.11) and (2.12). Now the integration is for the y domain $[y_1, 1]$. In scaled form we obtain

$$K_c = \frac{4}{3^4}\sqrt{2H}\left(\frac{1}{2Fr^3} - \frac{1}{5Fr^5}\right)A^5 t^{-4/3}, \tag{3.11}$$

$$P_c = \frac{4}{3^4 \times 5}\sqrt{2H}\,\frac{1}{Fr^5}A^5 t^{-4/3}, \tag{3.12}$$

$$E_c = K_c + P_c = \frac{2}{3^4}\frac{1}{Fr^3}\sqrt{2H}A^5 t^{-4/3}. \tag{3.13}$$

The conclusion is that the energy of the axisymmetric current in an $S = 1$ stratified ambient, at large times, decays like $t^{-4/3}$ or r_N^{-4}. In the self-similar stage $K_c > P_c$. In the present case $\mathscr{V} = 1/2$. This analytical result is in good agreement with the numerical solution of the SW equations. The decay of energy in the $S = 1$ stratified case is significantly faster than for the non-stratified $S = 0$ counterpart. We recall that this case corresponds to an intrusion which propagates along the plane of neutral buoyancy.

There is, again, a sharp difference between the axisymmetric self-similar behaviour for $S = 1$ and the two-dimensional counterpart. In the latter case $x_N \propto t^{1/2}$ (see Ungarish 2005*b*), and hence the energy decays like t^{-1} or like x_N^{-2}.

We have verified analytically for the self-similar solutions that $\mathrm{d}E_c/\mathrm{d}t$ is equal to the rate of pressure work performed by the nose. This is the mechanism by which energy is transferred from the current to the ambient fluid. The one-layer model does not predict how this energy is distributed in the ambient. However, the volume ratio of ambient to current is large, and hence this energy is so diluted in the ambient that it cannot affect significantly the assumed hydrostatic pressure field which embeds the current. This argument explains why the SW one-layer model is expected to remain a good approximation to the real motion in spite of the fact that a continuous and significant energy transfer to the ambient takes place from the beginning of the motion. The comparison with the NS results lends support to this interpretation.

The advantage of the self-similar results is that they can be applied to locks of various shapes by simply substituting the appropriate $\mathscr{V}$. For example, for an ellipsoid lock $h = \sqrt{1 - r^2}$ $(0 \leqslant r \leqslant 1)$, we use $\mathscr{V} = 1/3$ instead of $1/2$ for the cylinder. However, we keep in mind that some care is necessary in the practical use of the self-similar results. Since the initial conditions are not satisfied, these results are accurate for large times only. There are indications that the predicted trends are relevant after a spread to $r_N \approx 3$. On the other hand, we noticed that for large times the inviscid approximation becomes less valid. In any case, these effects affect the energy of the current in a consistent manner: a very fast decay is expected after propagation to $r_N \approx 3$. This conclusion is supported by the NS simulation discussed next.

3.2. *Navier–Stokes results*

The corresponding NS computations were performed on grids of 400×220 intervals. In these simulations $H = 3$ and $h_0/r_0 = 0.25$, $r_w = 8$, $Re = 9.62 \times 10^3$ and the values of S were $0, 0.29, 0.72$ and 1. The values of ϵ were $0.115, 0.115, 0.0804, 0.115$, respectively. These parameters were chosen so that the second and third cases reproduce axisymmetric counterparts of the experimental two-dimensional runs 5 and 19 of Maxworthy *et al.* (2002). Similar parameters were used in the previous study of the energy budgets in the two-dimensional case (Ungarish & Huppert 2006). The coefficient κ of the artificial smoothing term $\nabla^2\rho$ was grid-dependent, of the order of magnitude of the grid interval squared; in any case, $\kappa < 1/Re$, which corresponds to a Schmidt number $\sigma > 1$. (In real saline systems $\sigma \approx 10^3$, but this is beyond the resolution of the grids used in this work. However, since the Reynolds number is large, the value of the Schmidt number can influence only slightly the structure of the current. A recent investigation of this effect is presented in Bonometti & Balachandar 2008.)

Various verifications of the consistency and reliability of the numerical results were performed. These included changes of grid and time step, reduction of ϵ (to test the possible non-Boussinesq effects), and the reproduction of numerical results for $S = 0$ reported in Patterson *et al.* (2006). Results of earlier versions of this code also show fair agreement in comparisons with experimental data, see for example Hallwworth *et al.* (2001, figures 10, 13 and 15). Overall, we think that the numerical results are sufficiently reliable to provide support to the present investigation on energy transfer in the initial stage of propagation.

The propagation of the current is considered for the time (or distance) during which the influence of the wall at $r_w = 8$ can be neglected and during which the inertia effects are dominant. In contrast to the SW model, whose numerical solution required insignificant computer resources and the analysis of the data was straightforward, the NS simulation required significant CPU-time and storage space, and a large effort to process the data. (A typical simulation with our code ran for about 30 CPU-hours on a Sun V20z server, with processor 250, 2.4GHz, 4GB memory.)

Typical results of the NS simulations are shown in figures 7 and 8. We see that the shape of the current is very complex in the region of the nose. Stronger stratification (figure 8) reduces the height of the head compared to the case of weaker stratification (figure 7). The isopycnals of the ambient fluid are considerably displaced above the head of the current almost from the beginning of the process. (At advanced times the density contours also show significant perturbations near the axis $r < 0.1$, approximately, but the volume in this region is very small and hence this effect is unimportant.)

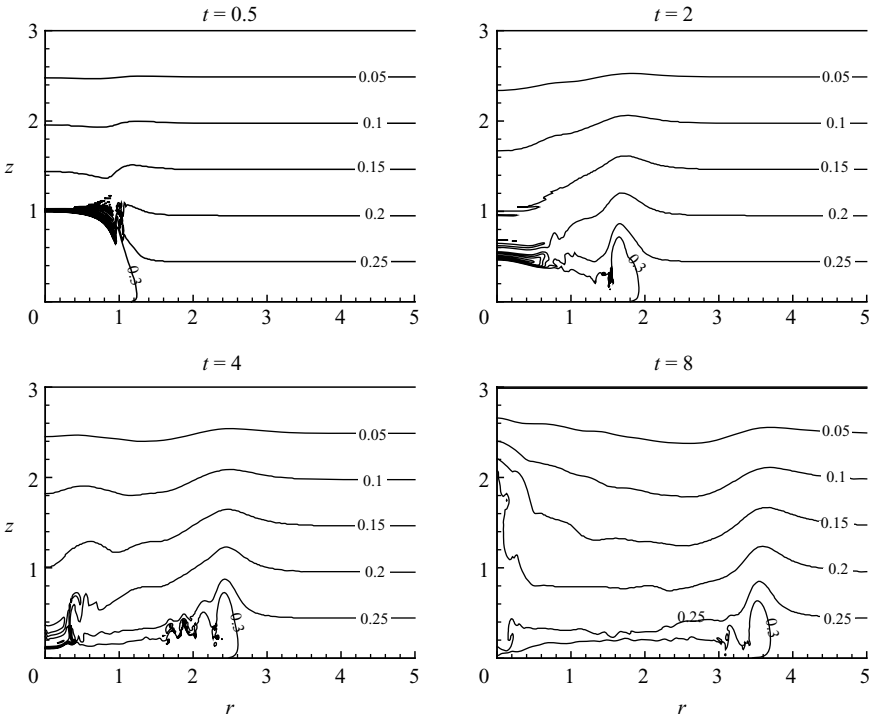

FIGURE 7. NS results. Density contour lines at various times for $S = 0.29$. The labels show the value of ϕ defined in (2.33).

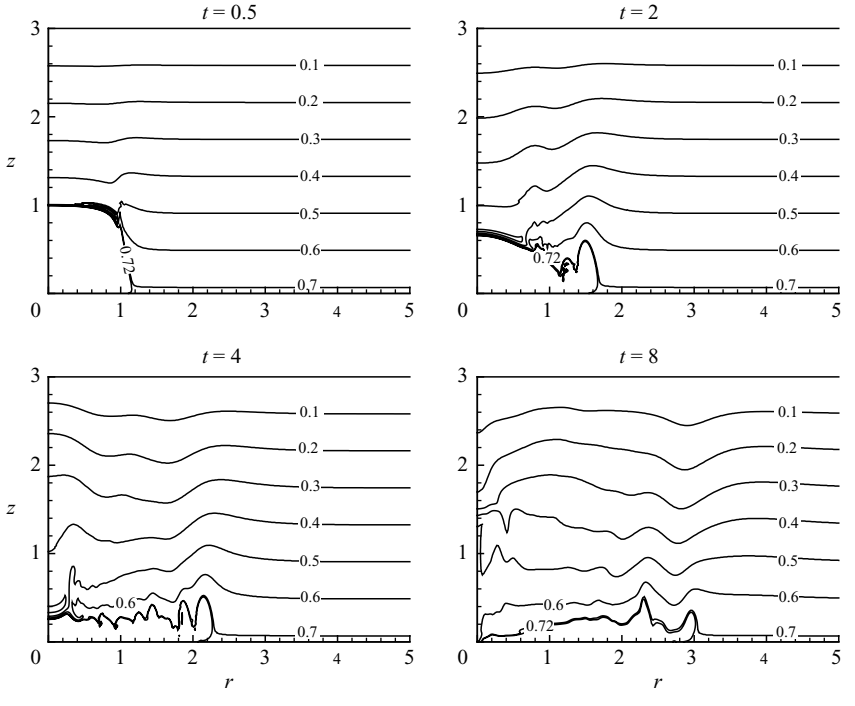

FIGURE 8. NS results. Density contour lines at various times for $S = 0.72$. The labels show the value of ϕ defined in (2.33).

The NS and SW predictions of the radius of propagation as a function of t are shown in figure 2. The agreement is good for initial times. Eventually, the NS results lag considerably behind the SW predictions. This can be attributed to the following effects. First, as previously mentioned, the axisymmetric NS simulations tend to lose accuracy and to underpredict the real propagation. As mentioned above, we verified the robustness of the results on different grids and time steps. The simulated current tends to disperse and lose coherence after propagation to about $r_N = 2.5$. We noticed that this effect is slightly reduced when the stratification and Re increase, and when ϵ decreases. This seems to indicate that shear-mixing about the nose generates some vortical motion which is numerically unstable in the axisymmetric geometry. This is consistent with the conclusions of Patterson *et al.* (2006). The implication is that the most severe discrepancy between the SW and axisymmetric NS results represents a deficiency of the latter solution rather than a limitation of the former approximation. This interesting relationship between the models has support for the unstratified case. Ungarish (2007) shows that the SW results are in good agreement with the experiments of Patterson *et al.* (2006) and Hallworth *et al.* (2001) for propagation to about $r_N = 6$, while the axisymmetric NS results show agreement only up to about $r_N = 3$. Cantero *et al.* (2007) also notes that SW models capture better the front velocity than highly resolved two-dimensional simulations. However, these conclusions still await confirmation for the stratified counterpart and intrusions. We also reiterate that three-dimensional high-resolution simulations are expected to resolve the deficiency of the axisymmetric (or two-dimensional) NS computations, but the computational cost is high and renders these verifications a topic for future work.

The second effect is that the propagation of the gravity current is hindered by effects which have not been incorporated in the SW model. This is further elucidated by comparing typical NS and SW profiles of the current. For the case $S = 0.72$, consider figures 4 and 9. We see that the NS-simulated current has a complex, wavy profile, with a prominent high head. The SW theory uses smooth profiles, with a sharp jump of the height from h_N to 0 at the nose. This difference justifies the larger drag and slower motion in the more realistic simulation. In spite of these discrepancies, it is clear that the SW approximation captures the effect of the stratification well.

To support the theoretical analysis, we verified the SW energy behaviour with the corresponding NS results. The pertinent comparison is shown in figure 10. We emphasize that the energies are normalized with the initial potential energy of the system, $P_c(0)$, given by (2.13). We observe that the SW and NS results are fairly close during the initial propagation. Eventually, the NS results decay more quickly to zero than the SW predictions. The agreement between the SW and NS potential energies of the current is better than that for the total energy of the current. This can be attributed to the same effects as the discrepancy observed for $r_N(t)$, because a slower propagation implies an even more significantly reduced kinetic energy. We conclude that, overall, the NS computations are consistent with the energy predictions of the simplified SW model. Again, the influence of the stratification is well captured. The graphs of figure 10 cover a fairly wide range of different systems. To illustrate this, let us apply these graphs to a fixed geometry and fixed densities of current ρ_c and at the top of the ambient ρ_o; we vary the stratification so that at the bottom ρ_b increases from ρ_o ($S = 0$) to ρ_c ($S = 1$). The unscaled initial potential energy for $S = 1$ is 9 times smaller than that of the unstratified, $S = 0$, counterpart. The initial speeds of propagation also differ by a factor of about 4. We find that for all these systems

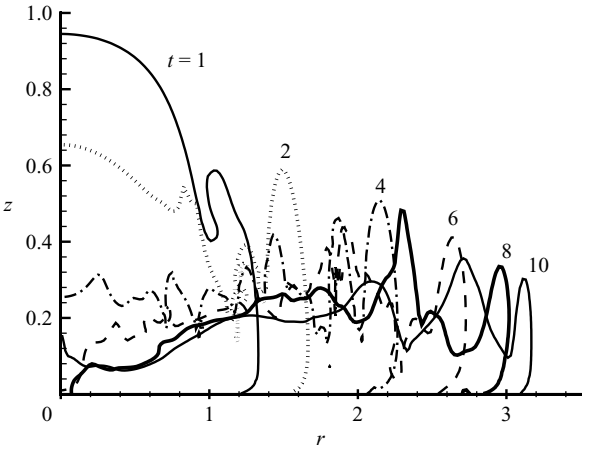

FIGURE 9. NS profiles of the current for $S = 0.72$, at various times.

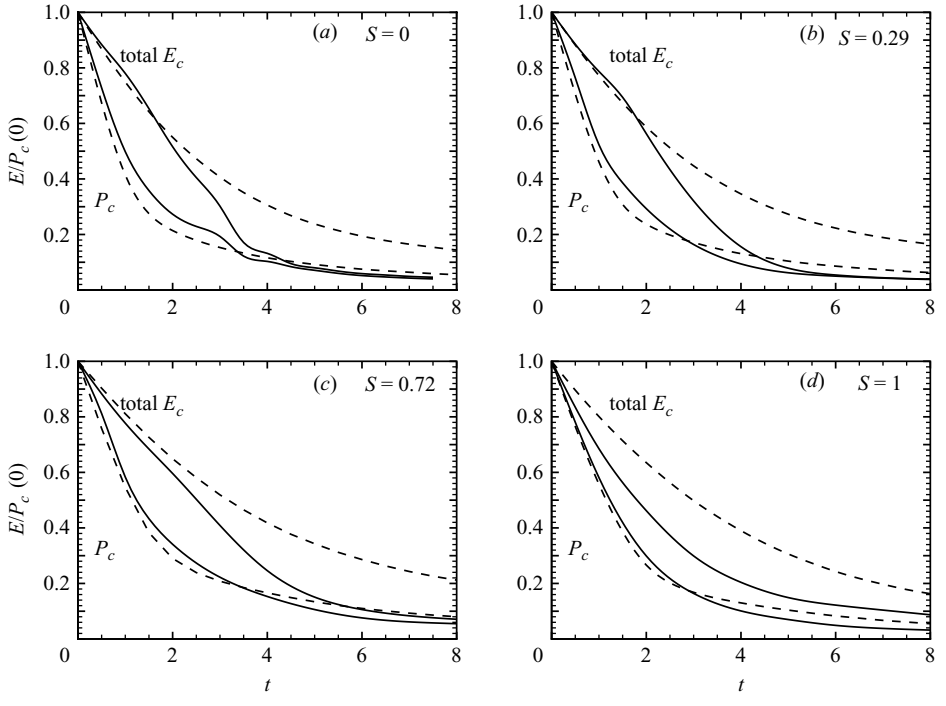

FIGURE 10. The potential and total (mechanical) energy of the current as functions of time. Comparisons of NS (full lines) and SW (dashed lines) results, for $S = 0$ (unstratified), 0.29, 0.72 and 1.0.

the SW model predicts the scaling and the trends of the energies of the current fairly well. This strengthens confidence in the general insights derived from the SW model about the effects of stratification.

Figures 11 and 12 provide information on the total mechanical energy (kinetic plus potential) of the two-fluid system and the energies of the ambient. This is obtained from the NS computations. Evidently, the total (mechanical) energy is not conserved

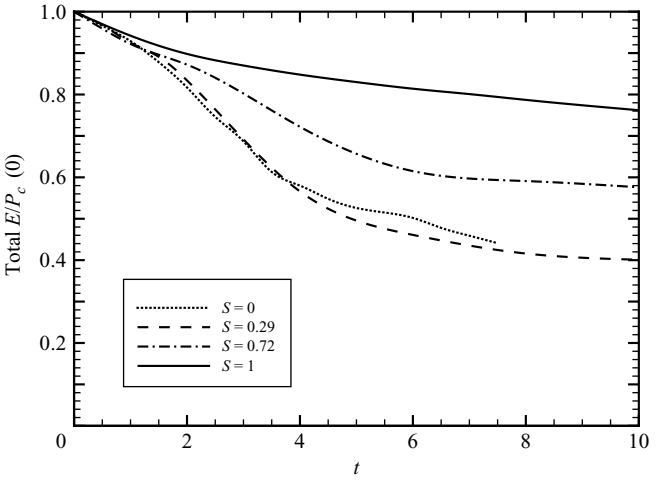

FIGURE 11. NS results for the total mechanical energy of the two-fluid system as a function of time for various S.

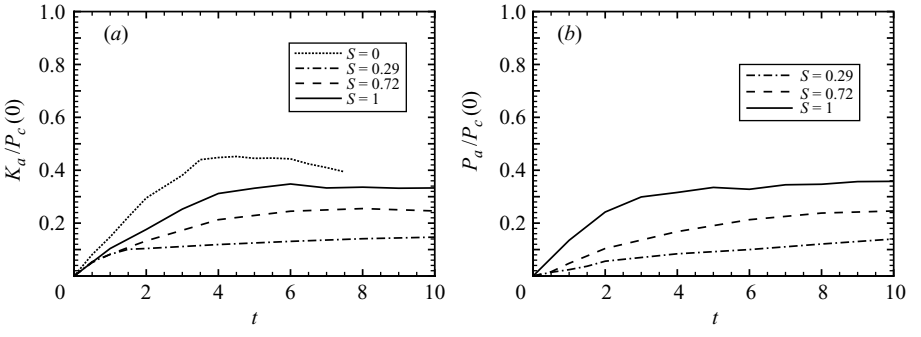

FIGURE 12. NS results for the kinetic (a) and potential (b) energy of the ambient as a function of time for various S. (The potential energy result for $S = 0$ is zero.)

because of irreversible viscous dissipation. We note that stratification hinders the decay of the total mechanical energy. The interpretation can be inferred from the behaviour of the kinetic and potential energies in the ambient. The stratification enhances the ability of the ambient to accumulate potential energy. Thus, as S increases, the ratio of kinetic to potential energy in the ambient is reduced. This reduces the velocity differences in the ambient field and hence also the viscous dissipative friction.

4. Concluding remarks

The shallow-water analysis presented here, which neglects motion in the ambient, seems to capture well the energy exchange of the axisymmetric gravity current in the inertia-dominated stage of propagation. In particular, this approach is able to elucidate by comparatively simple means the effects of stratification on the energy balances of the gravity current. It is somewhat surprising that the one-layer shallow-water model is relevant in spite of the fact that the ambient gains a significant part of the energy of the current. This can be attributed to two effects: (i) The energy transfer is a rather one-sided process. The current performs work on the ambient (mostly at the

propagating nose), and thus loses energy. From the point of view of the current, it is unimportant how this energy is further propagated. (ii) The volume of the ambient is large, and the initial disturbances there are zero. Consequently, when space and time averaged, the feedback to the current of the perturbations in the ambient are rather small for a significant distance of propagation.

In general, the trends of the energy budgets in the axisymmetric system are similar to those in the two-dimensional system (Ungarish & Huppert 2006). However, the transfers are more rapid in the diverging geometry: the axisymmetric current displays very sharp energy changes with radius of expansion, r_N (scaled with the initial r_0). When $r_N \approx 2$ the kinetic energy attains a maximum, and then both potential and kinetic energy decay: (*a*) like r_N^{-2} for a weak stratification; and (*b*) like r_N^{-4} for a strong stratification. The latter case is relevant to an intrusion at the neutral buoyancy level. As stratification increases, the capability of the ambient to store potential energy by the wavy displacement of the isopycnals increases. This reduces the portion of kinetic energy in the ambient and the friction dissipation.

We observed that the agreement between the predictions of the NS simulations and SW model is better for two-dimensional cases than for the axisymmetric counterpart. We think that this is due to a deficiency of the numerical finite-difference method used in the simulation, because previous studies (e.g. Patterson *et al.* 2006) reported similar discrepancies between NS simulations and experiments for the non-stratified case. This intriguing issue should be resolved by experiments and more sophisticated simulations. In this context we note that the three-dimensional high-resolution simulations of Cantero *et al.* (2007) provided good agreement with experiments for up to $r_N \approx 6$ in a full-depth lock release. Our expectation is that the more accurate data will show better agreement with the SW predictions than the present NS computations, and will sharpen the understanding of the process under discussion. These verifications require a great deal of additional work, which is left for the future.

We did not find a clear-cut difference between super- and sub-critical currents. We think that this is because in the axisymmetric case the speed of the nose decays from the beginning of the motion, and hence (*a*) in any case the sub-critical state prevails after a short propagation, and (*b*) when the interaction of the waves with the nose occurs (after a propagation of several lock lengths), the speed of the current is already so small that viscous effects dominate in our calculations. This is different from the two-dimensional geometry, in which the current propagates with constant speed for several lock lengths, and the interaction with the waves causes a dramatic reduction of the speed.

A major limitation of the SW energy balances used in our investigation is imposed by the neglected viscous friction. This effect cannot be easily incorporated into the analysis. We have presented a criterion for estimating the end of validity of the inviscid approach, but the understanding of the energy exchanges afterward requires a special investigation. Other deficiencies of the present SW model are the omission of the motion in the ambient and the development of three-dimensional structures for longer times. These topics are left for future work.

A comparison between the present results for the axisymmetric geometry and the previous results for the rectangular two-dimensional case (Ungarish & Huppert 2006) shows a similar quality of predictive power of the SW approximations. This indicates that, in spite of the above-mentioned restrictions, the SW model is a plausible and versatile tool which can be recommended for use in and extensions to other configurations.

The research was supported by an International Incoming Short Visits Royal Society grant to M.U. and a Royal Society Wolfson Research Merit Award to H. E. H.

REFERENCES

Amen, R. & Maxworthy, T. 1980 The gravitational collapse of a mixed region into a linearly stratified fluid. *J. Fluid Mech.* **96**, 65–80.

Baines, P. G. 1995 *Topographic Effects in Stratified Flows*. Cambridge University Press.

Benjamin, T. B. 1968 Gravity currents and related phenomena. *J. Fluid Mech.* **31**, 209–248.

Bonometti, T. & Balachandar, S. 2008 Effect of Schmidt number on the structure and propagation of density currents. *Theor. Comput. Fluid Dyn.* **22**, 341–361.

Cantero, M., Balachandar, S. & Garcia, M. H. 2007 High resolution simulations of cylindrical density currents. *J. Fluid Mech.* **590**, 437–469.

Faust, K. M. & Plate, E. J. 1984 Experimental investigation of intrusive gravity currents entering stably stratified fluids. *J. Hydraulic Res.* **22**, 315–325.

Flynn, M. R. & Sutherland, B. R. 2004 Intrusive gravity currents and internal gravity wave generation in stratified fluid. *J. Fluid Mech.* **514**, 355–383.

Grundy, R. E. & Rottman, J. 1985 The approach to self-similarity of the solutions of the shallow-water equations representing gravity current releases. *J. Fluid Mech.* **156**, 39–53.

Hallworth, M. A., Huppert, H. E. & Ungarish, M. 2001 Axisymmetric gravity currents in a rotating system: experimental and numerical investigations. *J. Fluid Mech.* **447**, 1–29.

Huppert, H. E. 2000 Geological fluid mechanics. In *Perspectives in Fluid Dynamics: A Collective Introduction to Current Research* (ed. G. K. Batchelor, H. K. Moffatt & M. G. Worster), pp. 447–506. Cambridge University Press.

Huppert, H. E. 2006 Gravity currents: a personal perspective. *J. Fluid Mech.* **554**, 299–322.

Huppert, H. & Dade, W. 1998 Natural disasters: Explosive volcanic eruptions and gigantic landslides. *Theor. Comput. Fluid Dyn.* **10**, 201–212.

Huppert, H. E. & Simpson, J. E. 1980 The slumping of gravity currents. *J. Fluid Mech.* **99**, 785–799.

Kao, T. W. 1976 Principal stage of wake collapse in a stratified fluid: Two-dimensional theory. *Phys. Fluids* **19**, 1071–1074.

Manins, P. C. 1976 Mixed region collapse in a stratified fluid. *J. Fluid Mech.* **77**, 177–183.

Maxworthy, T. 1980 On the formation of nonlinear internal waves from the gravitational collapse of mixed regions in two and three dmensions. *J. Fluid Mech.* **96**, 47–64.

Maxworthy, T. 1983 Experiments on solitary internal Kelvin waves. *J. Fluid Mech.* **128**, 365–383.

Maxworthy, T., Leilich, J. Simpson, J. E. & Meiburg, E. H. 2002 The propagation of gravity currents in a linearly stratified fluid. *J. Fluid Mech.* **453**, 371–394.

Morton, K. W. & Mayers, D. F. 1994 *Numerical Solutions of Partial Differential Equations*. Cambridge University Press.

Necker, F., Härtel, C. Kleiser, L. & Meiburg, E. 2005 Mixing and disipation in particle-driven gravity currents. *J. Fluid Mech.* **545**, 339–372.

Patterson, M. D., Simpson, J. E., Dalziel, S. B. & van Heijst, G. J. F. 2006 Vortical motion in the head of an axisymmetric gravity current. *Phys. Fluids* **18**, 046601.

Press, W. H., Teukolski, S. A., Vetterling, W. T. & Flannery, B. P. 1992 *Numerical Recipes in Fortran*. Cambridge University Press.

de Rooij, F. 1999 Sedimenting particle-laden flows in confined geometries. PhD thesis, DAMTP, University of Cambridge.

Schooley, A. H. & Hughes, B. A. 1972 An experimental and theoretical study of internal waves generated by the collapse of a two-dimensional mixed region in a density gradient. *J. Fluid Mech.* **51**, 159–175.

Shin, J. O., Dalziel, S. B. & Linden, P. F. 2004 Gravity currents produced by lock exchange. *J. Fluid Mech.* **521**, 1–34.

Simpson, J. E. 1997 *Gravity Currents in the Environment and the Laboratory*, 2nd Edn Cambridge University Press.

Stegner, A., Bouruet-Aubertot, P. & Pichon, T. 2004 Nonlinear adjustment of density fronts. Part 1. The Rossby scenario and the experimental reality. *J. Fluid Mech.* **502**, 335–360.

Ungarish, M. 2005*a* Dam-break release of a gravity current in a stratified ambient. *Eur. J. Mech.* B/*Fluids* **24**, 642–658.

Ungarish, M. 2005*b* Intrusive gravity currents in a stratified ambient-shallow-water theory and numerical results. *J. Fluid Mech.* **535**, 287–323.

Ungarish, M. 2006 On gravity currents in a linearly stratified ambient: a generalization of Benjamin's steady-state propagation results. *J. Fluid Mech.* **548**, 49–68.

Ungarish, M. 2007 Axisymmetric gravity currents at high Reynolds number – on the quality of shallow-water modeling of experimental observations. *Phys. Fluids* **19**, 036602/7.

Ungarish, M. 2008 Energy balances and front speed conditions of two-layer models for gravity currents produced by lock release. *Acta Mechanica*, (in press).

Ungarish, M. & Huppert, H. E. 1999 Simple models of Coriolis-influenced axisymmetric particle-driven gravity currents. *Int. J. Multiphase Flow* **25**, 715–737.

Ungarish, M. & Huppert, H. E. 2002 On gravity currents propagating at the base of a stratified ambient. *J. Fluid Mech.* **458**, 283–301.

Ungarish, M. & Huppert, H. E. 2004 On gravity currents propagating at the base of a stratified ambient: effects of geometrical constraints and rotation. *J. Fluid Mech.* **521**, 69–104.

Ungarish, M. & Huppert, H. E. 2006 Energy balances for propagating gravity currents: homogeneous and stratified ambients. *J. Fluid Mech.* **565**, 363–380.

Ungarish, M. & Zemach, T. 2007 On axisymmetric intrusive gravity currents in a stratified ambient - shallow-water theory and numerical results. *Eur. J. Mech.* B/*Fluids* **26**, 220–235.

Winters, K. B., Lombard, P. N., Riley, J. J. & D'Asaro, E. A. 1995 Available potential energy and mixing in density-stratified fluids. *J. Fluid Mech.* **289**, 115–128.

Wu, J. 1969 Mixed region collapse with internal wave generation in a density-stratified medium. *J. Fluid Mech.* **35**, 531–544.

Zemach, T. & Ungarish, M. 2007 On axisymmetric intrusive gravity currents in a deep fully-linearly stratified ambient: the approach to self-similarity solutions of the shallow-water equations. *Proc. R. Soc. Lond.* **463**, 2165–2183.